Journal of Coastal Research	22	6	1463–1473	West Palm Beach, Florida	November 2006

Hydrodynamics in a Mud Bank Regime during Nonmonsoon and Monsoon Seasons

R. Tatavarti[†] and A.C. Narayana[‡]

[†]Naval Physical & Oceanographic Laboratory
Defence R&D Organization
Thrikkakara
Cochin 682021, India

[‡]Department of Marine Geology & Geophysics
School of Marine Sciences
Cochin University of Science & Technology
Fine Arts Avenue
Cochin 682016, India

ABSTRACT

TATAVARTI, R. and NARAYANA, A.C., 2006. Hydrodynamics in a mud bank regime during nonmonsoon and monsoon seasons. *Journal of Coastal Research,* 22(6), 1463–1473. West Palm Beach (Florida), ISSN 0749-0208.

We present here an analysis of a set of measurements of water surface elevations (waves), cross-shore currents, and longshore currents from two cross-shore locations (at 50 and 200 m offshore) in the nearshore zone off Kerala, India, to understand the hydrodynamics in a mud bank regime. The measurements were made over a period of approximately one year to detect the differences in the nearshore hydrodynamic regime (*i.e.,* wave and current characteristics) between events of wind and wave activity during the nonmonsoon and monsoon seasons. A comparison of the data from the nonmonsoon season (when the water column was relatively free of suspended sediment load) and the monsoon season (when large suspended sediment load was present) showed significant differences in the hydrodynamic characteristics. During the nonmonsoon season, progressive edge waves in the infragravity frequency band with weak reflections were observed, while during the monsoon season, the presence of far infragravity waves, infragravity waves (leaky modes and trapped edge wave modes) coupled with strong shoreline reflections, and an undertow were observed. The nonlinear wave–wave interactions were noticed to be more pronounced in the upper water column, progressively diminishing vertically down toward the seabed and horizontally toward the shore. Based on the field observations and analysis, we present a plausible explanation for the formation, sustenance, and contraction of the mud bank.

ADDITIONAL INDEX WORDS: *Mud banks, southwest coast of India, gravity waves, edge waves, nonlinear wave interactions.*

INTRODUCTION

Mud banks are calm regions of nearshore seawater with very high concentrations of sediment in suspension, devoid of any significant wave action. They are found at only a few nearshore locations of the world oceans. They are known to occur on the southwest coast of India, especially off Purakkad in Kerala (Figure 1). It is generally known that the nearshore hydrodynamics of peninsular India are significantly affected by the monsoons. Of the two monsoons, the southwest monsoon (June–September) is the most active along the Kerala coast. The Kerala mud banks become more prominent with the onset of the southwest monsoon (*i.e.,* in the month of June), and less prominent at the end of the northeast monsoon (October–December) season. The mud banks of Kerala have socioeconomic effects because they are known: (i) for their very high biological productivity and (ii) for prevention of the otherwise rampant beach erosion during the southwest monsoon season. Coastal and ocean engineers believe that once the dynamics of mud banks are understood (*i.e., why* and *how* these nearshore phenomena form, sustain, and disappear), the knowledge can be applied to preventing coastal erosion and to increasing the productivity of the coastal oceans. The impetus for this study is the paucity of knowledge on mud bank dynamics, in spite of their socioeconomic importance.

Although a number of studies attempted to explain the formation, sustenance, and disappearance of the mud banks off Kerala, the phenomenon still remains an enigma (for reviews see FAAS, 1991, 1995; LI and PARCHURE, 1998; MATHEW and BABA, 1995; MATHEW, BABA, and KURIEN, 1995; MEHTA and JIANG, 1993; NAIR, 1976; SILAS, 1984; WELLS and KEMP, 1986). In hindsight this is not surprising, as most of the earlier studies on the Kerala mud banks covered basically their hydrographic features and the physical processes involved in their formation, but did not include real time, nearshore ocean monitoring. Even recent studies that addressed the problem of the mud banks of southwest coast of India attempted to suggest conceptually the formation, sustenance, and dissipation phenomena with no substantial field observations to support their hypotheses (JIANG and MEHTA, 1995; MATHEW and BABA, 1995). To the best of our knowledge no comprehensive field observations of mud banks were made.

DOI: 10.2112/05-0461.1 received 23 February 2005; accepted in revision 7 December 2005.

This study was sponsored by SERC, Department of Science & Technology (DST), Government of India under the project "Sediment dynamics and hydrodynamics of mudbanks off Kerala" (ESS/CA/A1-14/93).

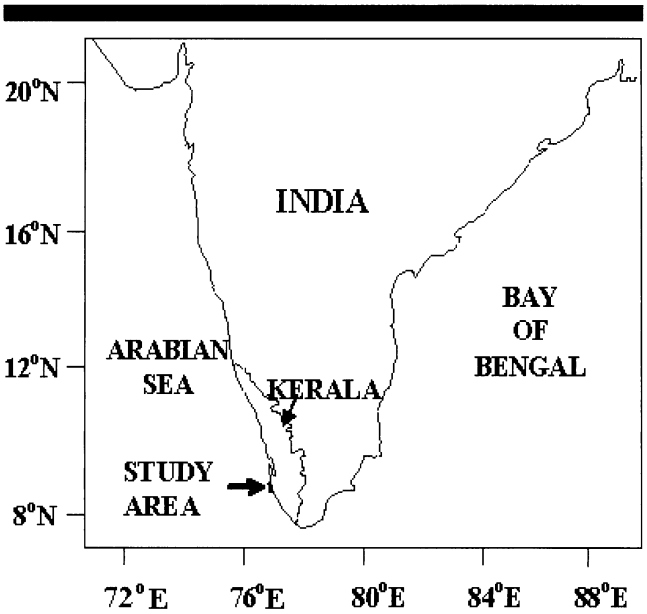

Figure 1. Location map of study area.

MATHEW and BABA (1995) measured only waves with a wave rider buoy (with an inherent low frequency cutoff at 0.05 Hz), completely neglecting the role of nearshore currents and undertow. Attempts to model the changing rheological characteristics of bottom mud in the mud bank region (JIANG and MEHTA, 1995) to explain the significantly high attenuation of monsoonal waves lacked proper parameterization from field observations. For example, the critical parameters of viscosity and shear modulus of the mud, required for their viscoelastic bottom mud model, were obtained from laboratory tests, which may not be representative of real field conditions. More recently, RODRIGUEZ and MEHTA (1998) suggested that based on laboratory investigations the shoreward streaming of mud under monsoonal waves is a plausible mechanism for mud bank formation with the onset of monsoon. LI and PARCHURE (1998) examined the physical factors influencing the suspended sediment concentration profiles and presented a semiempirical model that accounts for the vertical fluxes of fine sediment in suspension due to waves and currents. Their model simulations of suspended sediment concentration profiles were correlated with some of the field data from MATHEW and BABA (1995). The poor correlations between model simulations and the field data were attributed to be the result of the sparse and unreliable data.

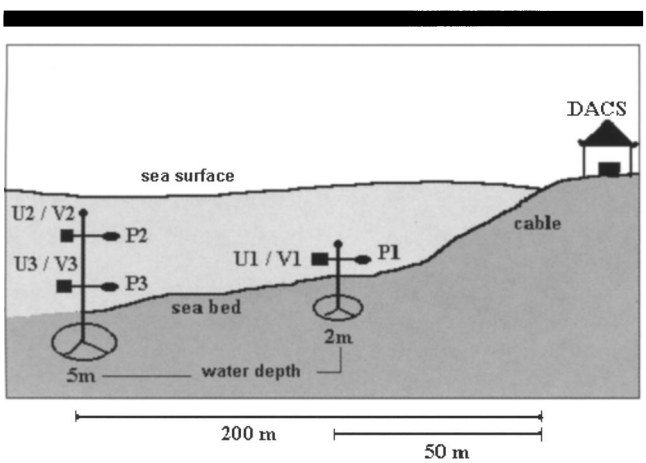

Figure 2. Schematic cross-sectional view of field experimental set up and sensor locations. P denotes pressure sensor, U denotes cross-shore current sensor, and V denotes longshore current sensor. The numerals denote different locations of the sensors. DACS refers to the shore-based data acquisition system. The two tripods supporting the sensors were placed at 2 and 5 m water depths.

Against this background of uncertainties in modeling, the suspended sediments coupled with the need for exhaustive field observations of nearshore waves and currents, we conducted field experiments in the nearshore region over a period of one year, at the prominent mud bank location, primarily to address the following questions:

(i) What are the nearshore hydrodynamics (wave and current characteristics) during nonmonsoon and monsoon seasons?
(ii) What are the mud bank dynamics (spatial extents and sediment characteristics) during nonmonsoon and monsoon seasons?
(iii) Are the nearshore hydrodynamics responsible for the mud bank formation, sustenance, and contraction? If so, *why* and *how*?
(iv) Can the mud bank conditions influence nearshore hydrodynamics?

FIELD EXPERIMENTS

Field experiments were conducted during the monsoon and nonmonsoon seasons by deploying standard pressure transducers and current meters off Purakkad, Kerala, in the nearshore waters of the Arabian Sea (Figure 1). The experiments were designed to ensure that nearshore wave and current data were recorded in different spatial and temporal domains, during calm and stormy sea conditions. The pressure transducers were inductance type, and the current meters were bidirectional drag force sensors, designed to record the current speeds in any aligned direction (*i.e.,* depending on the orientation of the current meter either the cross-shore component or alongshore component of the nearshore velocity may be monitored). Sensor calibrations were performed in a towing tank with a mechanized trolley and a random wave generation facility. Extensive intercomparisons with other available standard instrumentation were conducted to assess the performance of the sensors. During the calibration and intercomparison experiments, checks for the robustness and the sensitivity of the sensors were made. The response time of the pressure sensors and the current meters was found to be approximately 0.2 s, marginally different from the value of 0.1 s reported by the manufacturer. The frequency response of the pressure sensor was near unity between 0 and 2 Hz, while the frequency response of the current sensor was near unity between 0 and 5 Hz. The sensors were deployed in the ocean by fixing them on stable underwater platforms sitting on the seabed (Figure 2). The sensor locations were

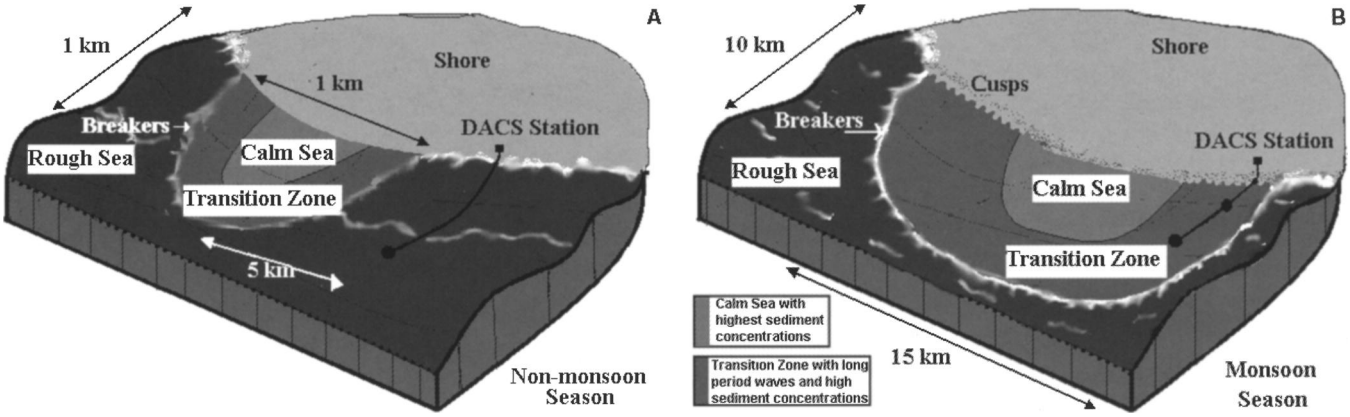

Figure 3. Schematic aerial view of the mud bank and location of sensors during the (A) nonmonsoon and (B) monsoon seasons. Note that the diagrams are not to scale. The scales shown in A and B are not the same either. **For color version of this figure, see page 1452.**

designed to capture the horizontal and vertical structure of the nearshore wave and current regime. Underwater coaxial cables were used to transmit signals between sensors in the ocean and the shore-based control unit. The analogue signals from the control unit were piped through an analogue-to-digital conversion (A-to-D) card into the shore-based computer to store real time digital data. The frequency and duration of data sampling were controlled on shore by the computer. Data were sampled at 2 Hz. Aerial surveys of the mud bank and its surroundings were conducted during field experiments from a helicopter to obtain a comprehensive picture in the spatial domain. During the aerial surveys, video recording was carried out using a Charge-Coupled-Device camera. Position fixing on board the helicopter during aerial surveys and on a small vessel during bathymetry survey was accomplished by using a portable global positioning system whose accuracy was ± 15 m.

During the field experiment in the monsoon season, the sensor pair (P1, V1/U1) was collocated on a platform at a height of 1 m from the seabed, in 2 m water depth. Sensor pairs (P2, V2/U2), and (P3, V3/U3) were deployed in 5 m water depth, fixed on a platform. Sensors (P2, V2/U2) were collocated at a height of 2 m from the seabed, while sensors (P3, V3/U3) were collocated at a height of 1 m from the seabed. The first platform in 2 m water depth was deployed at an offshore distance of 50 m from the shoreline, while the second platform in 5 m water depth was deployed at an offshore distance of 200 m from the shoreline. During the field experiments in the nonmonsoon season, only one platform (*i.e.,* at 5 m water depth) was deployed with collocated P, U, and V sensors at a height of 1 m from the seabed and another P sensor at a height of 2 m from the seabed. Because of the strong wave activity in the surf zone during the nonmonsoon season, the first platform could not be deployed with our existing logistic support.

VISUAL OBSERVATIONS

A seasonal waxing and waning of the mud bank region was observed. Figure 3 illustrates simple schematic representations of the mud bank and its relationship to the surrounding sea and is based on aerial surveys. Figure 3A shows the mud bank location relative to the sensor deployment during the nonmonsoon season; Figure 3B shows the mud bank location and size relative to the sensor locations during the monsoon season. During the nonmonsoon season, the mud bank spatial extents are generally much less—1 km in the cross-shore and longshore directions, while during the monsoon season, the periphery of the mud bank extends about 10 km seaward from the shoreline and stretches for about 15 km longshore.

Nonmonsoon Season

The spatial extents of the mud bank and the suspended sediment concentration in the mud bank region were observed to be rather small. During the nonmonsoon season the shoreline was generally straight, devoid of any cusps. Gravity waves were dominant and observed to be breaking shoreward of the outer sensor location. The surf zone was composed of plunging and collapsing breakers, with a width of 10–20 m. Wave reflections were observed to be rather weak. The significant wave heights were of the order of 1.5–2.5 m. Wave approach was predominantly from northwest. Whenever, the winds were strong (>50 knots), well-formed cusps with 15–20 m longshore spacing and heights of 0.5–0.7 m were observed.

Monsoon Season

The calm region was observed to be separated from the rough sea (significant wave height, $H_s \approx 2.5$ m) by a transition zone, where waves with longer wavelengths (low frequency infragravity waves) were observed to be dominant. The sediment concentration levels were greatest in the calm zone, decreasing progressively toward the rough sea. At the shoreline, the calm zone was observed to be bordered by a straight shoreline, while in the transition zone shoreline cusps were present (Figure 3B). The mud bank, which existed as a small patch in March, reactivated with the onset of the monsoon, gradually expanded and reached its maximum ex-

tension in both the cross-shore and longshore directions in October–November (NARAYANA, KUMAR, and TATAVARTI, 2001). The expansion of the mud bank was toward the south during the monsoon season. The extended size of the mud bank remained unchanged during the postmonsoon period but began to shrink at the end of the postmonsoon period, *i.e.*, from January. The mud bank region was seen to increase and decrease in size with changing wind conditions. Strong onshore winds were responsible for contraction of the mud bank and for the water inside the calm region becoming extremely turbid. These observations suggest that mud bank dimensions are controlled primarily by the prevailing meteorological conditions and the nearshore waves and currents. At the northern and southern boundaries of the mud bank, slowly propagating solitary waves were observed all the time. During the monsoon, the mud bank and the surrounding sea were observed to have significantly strong wave reflection. Surging and spilling breakers were observed in the transition zone, while plunging breakers were observed in the rough zone. The surf zone within the transition zone was narrow (≈10 m), while in the rough sea zone it was wide (≈ 50 m). During daily inspection of sensors at low tide, very strong longshore and cross-shore currents were observed with a relatively long periodic fluctuation (low frequency). The seabed was observed to have sinusoidal undulations (with vertical height of 5–10 cm and horizontal spacing of 1–2 m), slightly oblique to the shoreline. The beach cusp spacing in the transition zone, where the sensors were deployed, varied from 8.5 to 26.5 m with average vertical height of 0.5 m.

DATA FOR ANALYSES

In this paper, we focus on the role of mean currents, undertow, wave reflections, solitons, and nonlinearities in the nearshore wave and current dynamics during both the monsoon and nonmonsoon seasons, and their effects on the formation, sustenance, and contraction of mud bank are addressed. Therefore, representative wave and current data sets were selected from the monsoon and nonmonsoon seasons during varying wind and wave conditions. The primary reasons for choosing the specific data sets were as follows. (i) June 24, 1995: although calm meteorological conditions prevailed, a strong longshore current toward the north was observed. Also a very long data set (9-h duration) was recorded on that night, during which time the tide was ebbing; (ii) August 28, 1995: no significant wind activity was observed and the local sea was very calm; (iii) August 31, 1995: very strong winds were observed, the sea was choppy and there was a torrential downpour; (iv) September 1, 1995: very strong winds were observed, no rain was present but the sea became very choppy and the seaward boundary of the mud bank contracted toward the shore; (v) May 9, 1996: very strong wind and large waves were observed during the low tide as a local meteorological disturbance (depression) lay centered off the coast of Kerala. Table 1 summarizes the wave and current statistics of these data sets along with a brief description of the oceanographic conditions prevailing during the observations. The two specific data sets chosen for discussion in this paper pertain to (i) significant mud bank ac-

Table 1. *Statistics of water surface elevations and currents in mudbank regime during nonmonsoon and monsoon seasons.*

Date/Time	v/u	η Mean (m)	η Variance (m^2)	u Mean (m/s)	u Variance (m^2/s^2)	v Mean (m/s)	v Variance (m^2/s^2)	Remarks
May 9 at 1905 h	0.08	3.32	0.20	0.61 (shoreward)	0.03	−0.053 (southward)	0.021	Strong wind activity and predominant wave approach is from NW. Mostly 2-D waves having linear dynamics. Ebbing tide. Rough sea. Weak reflections. Nonmonsoon conditions.
June 24 at 2140 h	0.87	2.62	0.10	1.12 (seaward)	0.003	0.77 (northward)	0.017	Light to moderate winds. Waves approaching from NE. Ebbing tide. Strong reflections, undertow, longshore currents. Monsoon conditions.
Aug. 28 at 2330 h	0.62	2.99	0.02	−1.49 (seaward)	0.005	0.43 (northward)	0.002	No wind. No rain but overcast. Calm sea. Ebbing tide. Strong reflections, undertow, longshore currents. Monsoon conditions.
Aug. 31 at 1550 h	0.52	3.43	0.16	−1.35 (seaward)	0.001	−0.68 (southward)	0.018	Strong winds, Sea choppy White caps. Raining. Very long period waves. Harmonics. Rising tide. Strong reflections, undertow, longshore currents. Monsoon conditions.
Sept. 1 at 2230 h	0.77	3.08	0.09	−1.50 (seaward)	0.001	−0.79 (southward)	0.001	Monsoonal strong winds. Sea choppy, seaward boundary of mudbank at 600 m offshore. Rising tide, strong reflections, undertow, and longshore currents. Monsoon conditions.

tivity during the monsoon season (*i.e.,* August 31) and (ii) to the insignificant mud bank activity during the nonmonsoon season (*i.e.,* May 9). During the nonmonsoon season the sensors were in the rough sea (Figure 3A), not in the mud bank region because the mud bank was yet to reactivate and expand its peripheries, which had contracted significantly at the end of the previous monsoon season. During the monsoon season, however, the sensors were in the transition zone of the mud bank region with the incoming waves breaking seaward of the sensors (Figure 3B).

NEARSHORE WAVES, CURRENTS, AND UNDERTOW

Large amplitude wave group structures characteristic of two-dimensional wave dynamics (*i.e.,* with no longshore dependence), were observed during the nonmonsoon season, while small amplitude wave groups, characteristic of three-dimensional wave dynamics were observed during the monsoon season. Figure 4 shows representative time series of water surface elevation, η (demeaned and detrended), cross-shore (u), and longshore (v) currents (along with their means) during nonmonsoon and monsoon seasons. Gravity wave periods [O(10 s)] are more prominent in the water surface elevation, cross-shore, and longshore currents during the nonmonsoon season, while long period motions (>25 s) and very small period (<10 s) motions are prominent during the monsoon season. Cross-shore velocities of large amplitudes (~40 cm/s) with predominantly gravity wave periods during the nonmonsoon season, and slightly lower amplitudes (~20 cm/s) with predominantly long period oscillations (~1000 s) are evident during the monsoon season. The predominant direction of cross-shore current is shoreward during the nonmonsoon season and seaward during the monsoon season. The mean cross-shore current magnitude was ~60 cm/s, flowing shoreward during the nonmonsoon, and was ~130 cm/s, flowing seaward during the monsoon season. Assuming that the bulk seaward propagating mean flow is undertow, we point out that the monsoon season is characterized by a strong undertow.

The longshore velocity component shows predominantly gravity wave signatures with low amplitudes (~5 cm/s) having a southward direction in the nonmonsoon season, consistent with the fact that the position of the breaker zone was shoreward to the sensor location and that the predominant wind and waves approached from northwest. During the monsoon season, the longshore current shows very small period motions coupled with long period oscillations (having amplitudes of ~10 cm/s) with a predominant southward direction. The mean longshore current magnitude was much larger (~65 cm/s) during the monsoon season compared with that (~5 cm/s) of the nonmonsoon season.

Table 1 summarizes the statistics of water surface elevations and currents in the mud bank region during monsoon and nonmonsoon seasons under varying local environmental conditions. The data pertain to collocated sensors at a height of 1 m from the seabed in a water depth of approximately 5 m. The varying tidal conditions are reflected in the mean water surface elevation values, while the changing spectral energy levels of η, u, and v indicate the varying environmental conditions. The smaller $\langle v\rangle/\langle u\rangle$ ratio observed during nonmonsoon conditions suggests a lack of edge wave motions (HUNTLEY, GAZA, and THORNTON, 1981). Visual observations showed weak reflections during the nonmonsoon season, and strong wave reflections from the shoreline during the monsoon season. During the monsoon season under varying environmental conditions, the time averaged cross-shore current is significant and seaward flowing, indicative of a strong undertow. The significantly large $\langle v\rangle/\langle u\rangle$ ratio for observations during the monsoon, suggests the importance of edge waves in long period motions (HUNTLEY, GAZA, and THORNTON, 1981).

The variances associated with the time series of oscillations in Figure 4, are evident in the typical frequency spectra of water surface elevation (η), cross-shore current (u), and longshore current (v) from nonmonsoon and monsoon seasons shown in Figure 5. The spectra were computed from collocated sensors located at a water depth of 5 m and a height of 1 m from the seabed. The spectra were generated from consecutive 4096-s time series sections. Each section was detrended using a quadratic function (to remove tide) and demeaned before Fourier transformation. The 95% confidence levels are the same for all spectra for which computations were made using a 50% overlap Hanning spectral window having 60 degrees of freedom (dof) and a frequency resolution of 0.00048 Hz. The spectral frequency bands of the waves are marked as gravity (G) band [O(10^{-1} Hz)], infragravity (IG) band [O(10^{-2} Hz)], and far infragravity (FIG) band [O(10^{-3}–10^{-2}) Hz].

The most prominent feature during the nonmonsoon season is that the spectral energy levels are a maximum in the G band for water surface elevation and cross-shore and longshore velocity. The cross-shore velocity (u) also exhibits a peak in the FIG band. The features that stand out from the spectra of monsoon season are: (i) the low frequency variances in all spectra are larger, the far infragravity band in the elevation spectra having about an order of magnitude more energy than the gravity waves; (ii) longshore component (v) and cross-shore component (u) of nearshore velocity are stronger in FIG and IG bands; (iii) the gravity wave frequency band is least energetic.

The cross-spectral amplitudes, phases, and coherences between ηu, ηv, and vu during nonmonsoon and monsoon seasons were computed with more than 60 degrees of freedom. The upper 95% confidence level for coherence computations was 0.2. Table 2 shows the theoretical phase relationships between η, u, and v for different types of wave motions, after KIM, 1985; and the phase relationships between η, u, and v parameters with statistically significant coherence levels for representative data sets of nonmonsoon and monsoon seasons. Cross-spectral information from the η, u, and v sensors suggest linear dynamics of the gravity waves during nonmonsoon and monsoon seasons. During the nonmonsoon season, there is significant coherence between η and u and between η and v in the infragravity band, with η leading u when the two are in quadrature and η leading v when the two are in phase. There is relatively low coherence (although significant statistically) between v and u, with u leading v in

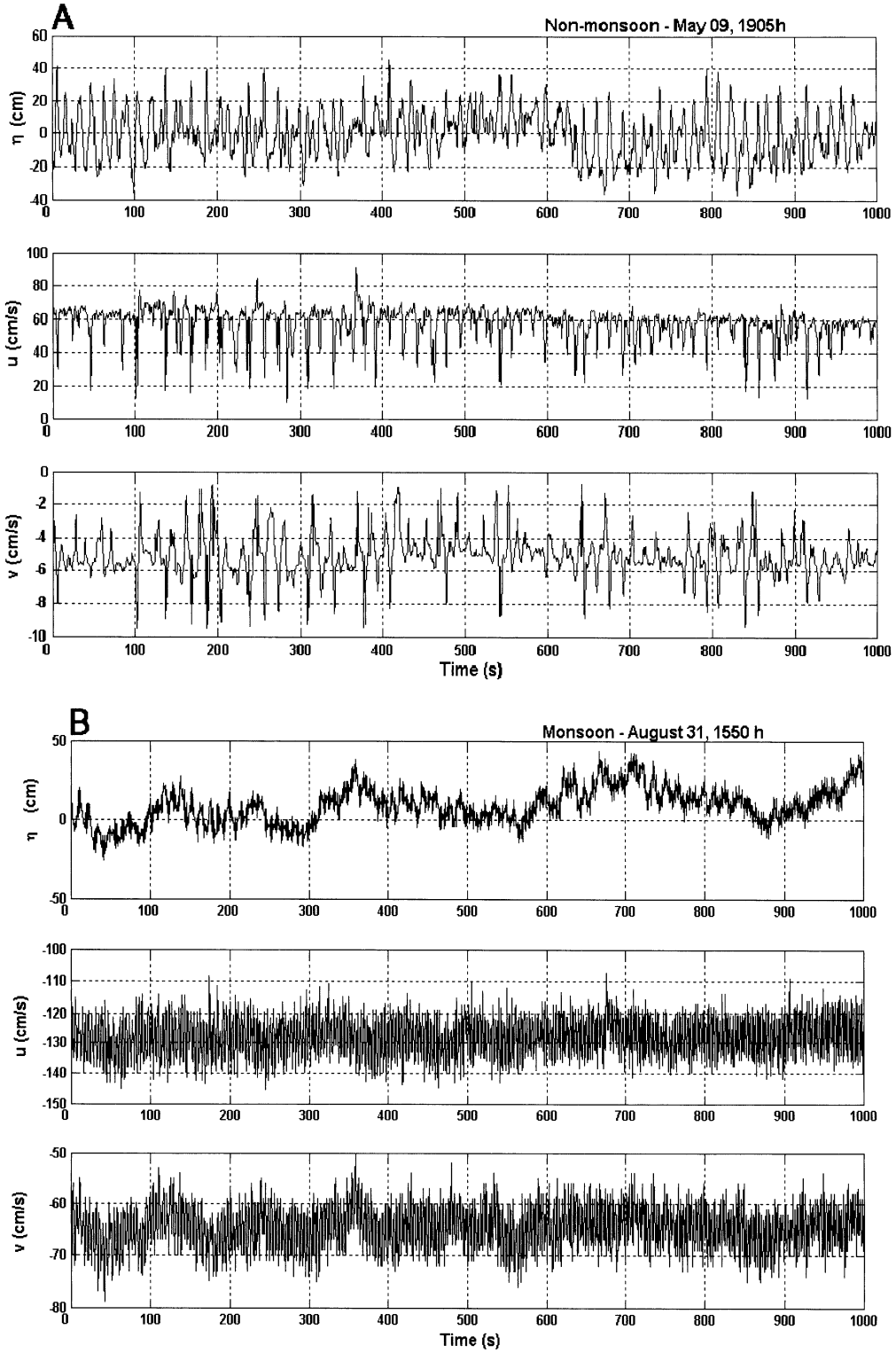

Figure 4. Representative time series of the measured water surface elevation (η [cm]), cross-shore current (u [cm/s]), and longshore current (v [cm/s]) during (A) nonmonsoon and (B) monsoon season. The negative values of u and v denote seaward and southward directions respectively. During the nonmonsoon season waves were breaking shoreward of the sensor location, while during the monsoon season waves were breaking seaward of the sensor location.

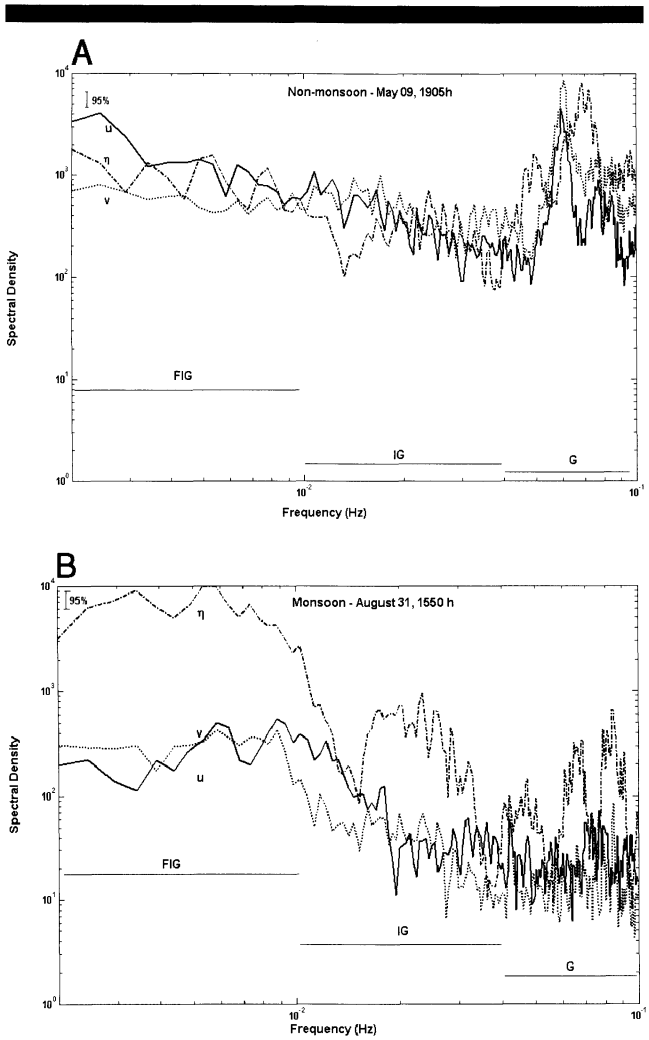

Figure 5. Spectra of water surface elevation (cm), cross-shore, and longshore currents (cm/s) during the nonmonsoon and monsoon seasons. The dof for spectral computations is 60 and the frequency resolution is 0.00048 Hz. The spectral frequency bands of the waves are denoted as the gravity (G) band [O(10^{-1} Hz)], the infragravity (IG) band [O(10^{-2} Hz)], and the far infragravity (FIG) band [O(10^{-3}–10^{-2}) Hz].

phase. In the FIG wave band significant coherence between η and v and between v and u was observed, with v leading η when they were in quadrature and u leading v when they were in phase. The coherence level between η and u was low, with η and u in quadrature, and η leading u. These observations suggest the presence of either standing wave motions or progressive edge waves in the nearshore (KIM and HUNTLEY, 1985; TATAVARTI, 1989). However, visual observations showed (Table 1, May 9, 1905 h) strong wind activity with weak reflections, thus ruling out the possibility of standing wave motions. Therefore we infer the presence of progressive edge waves in the infragravity frequency band. During the monsoon season it is observed that in the FIG band, the highest coherence is between η and u, with η leading u in quadrature. It is also found that in the FIG band, η leads v in quadrature while v leads u in quadrature. These results are consistent with the characteristics of FIG waves (OLTMAN-SHAY, HOWD, and BIRKEMEIR, 1989). The coherence in the IG band is also significant, but the coherence in the gravity wave band is not, except between η and u. In the IG band the highest coherence was found between the η–u pair and the u–v pair of series, although the coherence between the η–v pair is also significant. It can be noticed from Table 2 that in the IG band, η leads u and v when they are in quadrature, while v leads u when these two are in phase. These features in the IG band are consistent with standing edge wave dynamics (KIM and HUNTLEY, 1985). The indication of edge waves in the present data, coupled with the visual observation of shoreline cusps during that time is consistent with some of the earlier theories suggesting a link between infragravity motions and beach cusps (for *e.g.,* BOWEN and HUNTLEY, 1984; SALLENGER, 1979).

A comparison of Figures 4 and 5 and of Tables 1 and 2 reveal some of the pertinent differences in hydrodynamics between nonmonsoon and monsoon seasons. During the nonmonsoon season, gravity waves are dominant, while during the monsoon season low frequency waves dominate the nearshore dynamics. The ratio of the longshore current to the cross-shore current is smaller during the nonmonsoon season and larger during the monsoon season. In addition during the nonmonsoon season the energy levels (η, u, and v) in the gravity and infragravity bands were larger than those during monsoon season, while the energy levels of η, u, and v for the FIG band was observed to be higher during the monsoon season. That the variance in η is larger by an order of magnitude compared with that in the u and v components in the FIG band suggests the role of stronger FIG waves. Based on data observed during the monsoon season, it was established that the cross-shore velocity in the FIG band was larger near the ocean bottom compared with that in the middle of the water column, indicative of a strong undertow (PUTREVU and SVENDSEN, 1993).

COLLOCATED PRESSURE, VELOCITY CROSS-CORRELATIONS, AND SPECTRAL COHERENCES

During the nonmonsoon season when the waves were breaking shoreward of the 200-m offshore location, the cross-correlation peak for the vertically separated sensor pair (P2, P3) was 0.9 with P2 leading P3 at zero lag, while the peak cross-correlation was −0.25 for the collocated sensor pair (P3, U3) with U3 leading P3 at zero lag, and the zero frequency spectral coherence value was observed to be 0.15.

During the monsoon season when the waves were breaking seaward of the sensor location, a cross-correlation of surface elevations and cross-shore current velocity revealed that for the collocated but vertically separated sensor pair (P2, P3 in Figure 2) the peak cross-correlation coefficient was 0.75, with P2 leading P3 at zero lag. For the collocated (P3, U3 in Figure 2) sensor pair deployed at 200 m and closer to the seabed, the cross-correlation peak was −0.1 with P3 leading U3, with a time lag of 75 s. For the horizontally separated sensor pair (P3, P1 in Figure 2) the peak cross-correlation coefficient was 0.8 with P3 leading P1, with a time lag of 25 s.

Undertow is considered as the average offshore return flow

Table 2. *Phase relationships for different wave motions.*

Theoretical u, v, η phase relationships (after KIM, 1985)				
Wave	η-u		η-v	v-u
Progressive wave	In phase		In phase	In phase*
Standing wave	Quadrature		In phase	Quadrature*
Progressive edge wave	Quadrature		In phase	Quadrature
Standing edge wave	Quadrature		Quadrature	In phase
Spectral Frequency Band	η-u Cross-Spectral Phase	η-v Cross-Spectral Phase	v-u Cross-Spectral Phase	Remarks
Spectral characteristics of the hydrodynamis during nonmonsoon season				
G	In phase	In phase	In phase	No lead or lag between η, u, v
IG	Quadrature	In phase	Quadrature	η leads u, η leads v, and u leads v
FIG	Quadrature	Quadrature	In phase	η leads u, v leads η, and u leads v
Spectral characteristics of the hydrodynamics during monsoon season				
G	In phase	In phase	In phase	No lead/lag between η, u, v linear phase between v and u indicative of travel time associated with distance of separation
IG	Quadrature	Quadrature	In phase	η leads u, η leads v, and v leads u
FIG	Quadrature	Quadrature	Quadrature	η leads u, η leads v, and v leads u

G, Gravity waves (0.04–0.1 Hz); IG, infragravity waves (0.01–0.04 Hz); FIG, far infragravity waves (0.001–0.01Hz).
* For near normally incident waves, v could be small resulting in low coherence.

below the wave trough level, which balances the mass flux carried shoreward by wave breaking. The mass flux significantly increases the vertical nonuniformity of the wave radiation stress with much higher values between wave trough and crest levels. The smaller (~0.1) cross-correlation peak between the collocated pair (P3, U3) time series at a time lag of 75 s is consistent with the predicted time travel for the shoaling waves to travel the distance from the sensor location to shoreline and back. Also, the near zero frequency (P3, U3) spectral coherence value was observed to be 0.7, suggesting the presence of a bottom return mean flow. The spectral coherence values for the gravity wave frequencies were found to be approximately 0.1 only. This is in contrast to the linear gravity wave dynamics where (i) the cross-correlation between collocated (P, U) sensor series would have shown a large magnitude at zero time lag, and (ii) a low spectral coherence value at lower frequencies with closer-to-unity coherence values in the gravity wave frequencies are expected. From the aforementioned observations, and the observation of a strong (~130 cm/s) seaward flowing mean current, we infer a significantly strong undertow during the monsoon season. Because the spectral differences between collocated pressure and velocity estimates may be an artifact of the nonlinear wave dynamics (GUZA and THORNTON, 1980) we infer linear wave dynamics during the nonmonsoon and nonlinear wave dynamics during the monsoon seasons.

WAVE REFLECTIONS

Naturally occurring frequency dependent shoreline reflections were computed following the noise free technique developed by TATAVARTI (1989) and validated by HUNTLEY, SIMMONDS, and TATAVARTI (1999) utilizing time series measurements of collocated η and u measurements. TATAVARTI (1989) showed that frequency dependent wave reflection coefficient $R(\omega)$ can be computed using the relation:

$$R(\omega) = \frac{\sqrt{1 + G^2(\omega) - 2G(\omega)\cos\,\theta_{\eta u}(\omega)}}{\sqrt{1 + G^2(\omega) + 2G(\omega)\cos\,\theta_{\eta u}(\omega)}}$$

where ω is the wave frequency, G the gain function between the spectral amplitudes of elevation η and the current velocity u, and $\theta_{\eta u}$ is the spectral phase angle between η and u. By using principal component analysis to separate the current and elevation time series into orthogonal eigenvector combinations, TATAVARTI (1989) and HUNTLEY, SIMMONDS, and TATAVARI (1999) demonstrated that the first eigenvector would tend to extract the correlated part of the signals leaving any noise predominantly in the second and higher eigenvectors. Application of TATAVARTI's (1989) technique showed that wave reflection was very weak during the nonmonsoon season, consistent with the observation that the gravity wave band was highly energetic with waves breaking significantly before reaching the shore. During the monsoon season, the computed wave reflections in all frequency bands were large (>0.6), the maximum (0.8) being in the lower frequencies. Our visual observations of seabed undulations are in sync with the computed strong reflections, indicating that the seabed undulations may have been generated by the strong standing wave motions on the beach.

NONLINEAR WAVE INTERACTIONS— BISPECTRAL ANALYSIS

Bispectral analysis is a useful tool for examining time series for wave–wave nonlinear interactions leading to quadratic phase coupling and thus skewness. For the nonmonsoon season we looked at the bispectral analysis of water surface elevation data from the vertically separated P2 and P3 sensors, when waves were breaking shoreward of this location. To examine the role of the spatial evolution of nonlinearities during the monsoon season, we resorted to a bispectral analysis of the wave data from two vertically sepa-

Table 3. *Bicoherence of wave elevations during monsoon and nonmonsoon seasons.*

Data Run And Sensor Location Details	Interacting Frequency Pairs (ω_1, ω_2)	Bicoherence Peak Value
May 9, 1905 h, nonmonsoon		
1. P2, 200 m offshore, 5 m water depth at 2 m above seabed	(0.01, 0.01)	0.34
2. P3, 200 m offshore, 5 m water depth at 1 m above seabed	(0.01, 0.01)	0.11*
August 31, 1550 h, monsoon		
3. P1, 50 m offshore 2 m water depth at 1 m above seabed	(0.22, 0.22)	0.56
4. P2, 200 m offshore, 5 m water depth at 2 m above seabed	(0.02, 0.02)	0.30
	(0.02, 0.22)	0.25
	(0.11, 0.11)	0.24
	(0.22, 0.22)	0.80
5. P3, 200 m offshore, 5 m water depth at 1 m above seabed	(0.02, 0.02)	0.30

* Statistically not significant

rated sensors (P2 and P3) at 200 m offshore location; and from the P1 sensor, horizontally separated from P2 and P3 in the cross-shore direction at 50 m offshore location. To identify significant phase-coupled modes, we expressed the bispectrum in a normalized form known as the bicoherence spectrum. Bicoherence is defined as $\beta(\omega_1, \omega_2)$,

$$\beta(\omega_1, \omega_2) = \frac{|B(\omega_1, \omega_2)|}{\{E[|C(\omega_1)C(\omega_2)|^2]E[|C(\omega_1 + \omega_2)|^2]\}^{1/2}}$$

where $B(\omega_1, \omega_2) = E[C(\omega_1)C(\omega_2)]C^*(\omega_1 + \omega_2)]$ is the bispectrum, $E(x)$ is the expected value of x, and $C(\omega)$ is the complex Fourier coefficient at frequency ω (ELGAR *et al.*, 1995). For the bicoherence normalization used here, the 95% significance level for zero bicoherence is given approximately by (6/degrees of freedom)$^{1/2}$ (ELGAR and GUZA, 1988). Significant bicoherence indicates frequency pairs (ω_1, ω_2) that are involved in either sum or difference triad interactions (ω_1, ω_2, $\omega_1 + \omega_2$). The 95% significance level of bicoherence is approximately 0.21; therefore only bicoherence values above 0.21 are statistically significant. The bicoherence estimates for water surface elevation data at different locations are shown in Table 3. The frequency components of the significant bicoherence peaks for the nonmonsoon season are (0.01 Hz, 0.01 Hz) and for the monsoon season are (0.02 Hz, 0.02 Hz), (0.02 Hz, 0.22 Hz), (0.02 Hz, 0.02 Hz), (0.11 Hz, 0.11 Hz), (0.22 Hz, 0.22 Hz) suggesting self–self interactions and sea–swell interactions between two principal frequency components and their harmonics. During the monsoon season, as the waves approach the shore (from the 200 to 50 m location) the bicoherence of components (0.22 Hz, 0.22 Hz) was observed to reduce significantly from 0.8 to 0.56. Looking at the vertical variation in the water column at 200 m location, the bicoherence (0.8) of components (0.22 Hz, 0.22 Hz) was observed to be stronger at the top of the water column compared with the bicoherence (0.3) of components (0.02 Hz, 0.02 Hz) close to the seabed. Bicoherence estimates suggested that the nonlinear generation of increasingly higher frequencies due to wave–wave interactions was more dominant at 200 m offshore in the upper water column and had considerably diminished toward the seabed and also as the waves approached shore. The self–self interactions are known to generate first harmonic frequencies, *i.e.,* a second-order Stokes-type nonlinearity, and leads to positive velocity skewness. For the sea–swell interactions, sum and difference frequency interactions are possible, and the resulting velocity skewness can be negative (CRAWFORD and HAY, 2001). The contributions arising from phase coupling between wind wave and infragravity wave frequencies suggest that a given triad interaction within the (ω_p, ω_Δ) peak (where ω_p denotes the spectral peak frequency and ω_Δ denotes the beat frequency) indicates that the two primary wave trains are phase coupled to a long wave. We did find evidence of coupling between long waves and wave groups by looking at the cross-correlations between the two time series from the nonmonsoon season. During the monsoon season, wave groupiness was not significant (wave breaking was seaward of the sensor location), although the low frequency waves were dominant. In summary the bicoherence estimates were found to decrease shoreward and increase upward in the water column.

MUD BANK FORMATION, SUSTENANCE, AND CONTRACTION

Our earlier studies (MANOJKUMAR, NARAYANA, and TATAVARTI, 1998; NARAYANA, KUMAR, and TATAVARTI, 2001; TATAVARTI *et al.*, 1999) indicated the presence of fine sediments (predominantly clayey silts) blanketing the seabed during both monsoon and nonmonsoon seasons, even though the beach was primarily composed of sand. The thickness and concentration of surficial fine sediments blanketing the seabed, however, varies with seasons and wave regimes. The silt–clay ratio of the surficial sediments is greater during the stormy monsoon season than during the calmer nonmonsoon season; *i.e.,* finer sediments blanket the seabed during calmer sea conditions and coarser sediments blanket the ocean during rough monsoon season. Thus the mud bank regime is very unique because the coast is sandy with no major rivers debauching sediments into the sea, but the sediments in suspension and those blanketing the seabed are cohesive clayey silts. This further begs the question whether the pertinent physics and nearshore sediment dynamics are dictated by the sandy sediments on the coast or the cohesive sediments in suspension and on the seabed. Our field observations suggest that the hydrodynamics are similar to those of sandy beaches while the sediment dynamics are governed by cohesive sediments; *i.e.,* the suspension and movement of cohesive sediments are governed by fluid flows similar to those found on sandy coasts.

It is well known that the resuspension and movement of cohesive sediments by fluid flows can be studied using comprehensive numerical models whose principal mechanistic ingredients should include waves, wave-induced currents, and time-averaged mean currents. While the existing models have become quite sophisticated in computational terms and in the turbulence modeling aspect, they still depend on numerous calibration parameters that must be extrapolated from limited field measurements. Many uncertainties not ac-

counted for by these turbulence models remain. For example, the bed boundary condition is still based largely on laboratory experiments for steady flows. The dependence of fall velocity on coagulation and flocculation of cohesive sediments, and the effects of consolidation on the threshold stress are important issues that still remain unresolved. In most numerical models the role of waves is vastly oversimplified and is limited to being the source for imparting the shear stress required for sediments to cross the critical threshold into suspension. However, it is now established that waves play a significant role in enhancing the long term convection and diffusion of sediments in the wave boundary layer, where sediment concentrations are greatest. MEI, FAN, and JIN (1997) demonstrated that in addition to sediment resuspension, waves can also move the highly concentrated fluid mud, which is known to behave as a non-Newtonian fluid; in particular, through second order Reynolds stresses, waves generate a streaming velocity that varies horizontally with the scale of the wavelength. Thus there is clearly a need for a theoretical model encompassing the coupled movement of waves and fluid mud, as well as erosion and deposition of sediments near the bottom. Moreover, as suggested by MEI, CHIAN, and YE (1998), the effective horizontal diffusion is magnified by the vertical shear in the bottom boundary layer. This magnification can be very significant because the tidal period is very long compared with the wave period, resulting in a dispersivity that is much greater than the eddy diffusivity. Because the flow inside the boundary layer is determined by the flow above, which in turn is affected by the bathymetry and the coastline geometry, the effective diffusivity and convection velocity are dictated by the overall nonuniformity of the flow field and must, in general, vary from place to place. This means, in particular, that the dispersivity coefficients cannot be regarded as empirical constants to be calibrated by a few field measurements at a few locations.

The results from field experiments, conducted during the monsoon season, clearly indicated that the infragravity (IG) waves (*leaky modes and trapped edge wave modes*) and far infragravity (FIG) waves together with a strong undertow play an important role in the dynamics associated with the mud banks. During the monsoon season the waves were observed to be breaking at the offshore periphery of the mud bank region, at an offshore distance of 1 to 5 km from the shore. Many researchers (AAGAARD, GREENWOOD, and NELSON, 1997; BOWEN and HOLMAN, 1989; OLTMAN-SHAY, HOWD, and BIRKEMEIR, 1989; SHRIRA, VORONIVICH, and KOZHELUPOVA, 1997) have argued that the presence of FIG waves or shear instabilities may be an artifact of the pulsating cross-shore mean currents and the strong longshore current component. Our observation of the significantly stronger FIG wave activity (Figure 5B) shoreward of the breaking zone, where the surf zone width was of the order of kilometers with presumably strong bottom friction and eddy viscosity, is contradictory to the belief (FALQUES, IRANZO, and CABALLERIA, 1994) that the number of possible unstable modes and their growth rates may be reduced by dissipation because of bottom friction and eddy viscosity. We point out that the role of bottom friction and eddy viscosity on the growth of shear instabilities is yet to be realistically modeled.

Therefore in the absence of any realistic model for explaining the dynamics of mud banks (formation, sustenance, and contraction), we infer the following based on field observations. As waves start building up during the monsoon season, more and more of the sediments blanketing the seabed are placed in suspension. The suspended sediments are dispersed by the stronger littoral currents, infragravity and far infragravity wave regimes coupled with the strong reflections and undertow—thus extending the spatial extents of the mud bank in the longshore and cross-shore directions. As the wind and wave activity subside, the reverse of these processes takes place, resulting in the contraction of the mud bank extents and the decrease in the suspended sediment load. In other words, the sediments blanketing the seabed increase and decrease in thickness with the decrease and increase of wave activity.

We surmise that the smaller bicoherence values near the seabed may be an artifact of the viscous damping nature of the water column because of the presence of the thick sediment blanket. This coupled with the presence of a strong undertow may be the reason why solitons were observed at the longshore boundaries of the mud bank region, where we presume that the sediment blanket would have been instrumental in enforcing a balance between wave nonlinearities and wave dispersion, resulting in the generation of solitons.

CONCLUSIONS

The mud bank is a calm patch of water adjoining the coastline with a surrounding rough sea. The calm region is devoid of any wave activity with a very high load of suspended sediments. The mud bank's spatial extent is strongly influenced by the local meteorological conditions and the ensuing nearshore hydrodynamics. Field experiments in the mud bank during nonmonsoon and monsoon seasons provided a comprehensive picture of the nearshore hydrodynamics.

During the calmer nonmonsoon season the predominant waves are gravity waves. The wave heights are smaller in and around the mud bank region because of the weak wind forcing. Consequently, the littoral current regime and undertow are also weak. The smaller waves tend to break closer to the shoreline. The smaller breaking waves trigger far less sediment into suspension. The mud bank region is very limited in its spatial extent because the wave breaking occurs predominantly closer to the shore and the littoral currents are weaker. Local meteorological disturbances could, however, generate larger waves, which dissipate once the disturbance diminishes.

With the onset of the monsoon season, the wind forcing picks up, the wave heights start increasing and the sea gradually becomes rough. The rough sea conditions enable larger waves to start breaking at higher water depths (*i.e.,* the breaking zone shifts seaward). This means that there would be a stronger propensity for the sediments on the seabed to be triggered into suspension from a further seaward location. The larger waves ensure higher concentrations of sediments into suspension. During the rough monsoon season, in addition to the gravity wave band, the low frequency (infragravity and far infragravity) wave bands also become energetic.

Therefore, the littoral currents and the undertow also become stronger because they are primarily driven by the nearshore wave regime. As the monsoon season progresses, the low frequency motions (three-dimensional motions with both cross-shore and longshore dependence) become much more pronounced than the gravity waves inside the mud bank region. This is because the region acts as a dissipater of gravity waves because of the high concentration of suspended sediments in the water column. Because of their longer wavelength and therefore lower steepness, the low frequency waves do not break. Hence the degree of wave reflection also increases. The strong undertow and the reflected waves tend to push the sediment blanket on the seabed seaward. Therefore the seaward breaking waves would impart their energy to trigger this sediment layer into suspension. This ensures that the offshore extent of the mud bank shifts seaward. The seaward breaking waves, stronger littoral currents, and undertow, coupled with the stronger low frequency wave motions with their cross-shore and longshore dependence, therefore ensure that the spatial extents of the mud bank region increase during the monsoon season. As the monsoon season ends, the strength of the wind and hence the waves subsides. This ensures that the breakers approach shoreward resulting in a contraction of the mud bank.

ACKNOWLEDGMENTS

Doctor K.R. Gupta, DST; Director, NPOL, is acknowledged. Sincere thanks to Professor B. Greenwood, University of Toronto; Professor D.A. Huntley, University of Plymouth; Professor R.W. Sternberg, University of Washington; Dr. J. Oltman-Shay, NWRA; Professor A.J. Mehta, University of Florida, and the anonymous referees.

LITERATURE CITED

AAGAARD, T.; GREENWOOD, B., and NIELSEN, J., 1997. Mean currents and sediment transport in a rip channel. *Marine Geology,* 140, 25–45.

BOWEN, A.J. and HOLMAN, R.A., 1989. Shear instabilities of the mean longshore current: (1) Theory. *Journal of Geophysical Research,* 94(C12), 18023–18030.

BOWEN, A.J. and HUNTLEY, D.A., 1984. Waves, long waves and nearshore morphology. *Marine Geology,* 60, 1–13.

CRAWFORD, A.M. and HAY, A.E., 2001. Linear transition ripple migration and wave orbital velocity skewness: observations. *Journal of Geophysical Research,* 106(C7), 14113–14128.

ELGAR, S. and GUZA, R.T., 1988. Statistics of bicoherence. *IEEE Transactions of Acoustics Speech, Signal Processing,* 365, 1667–1668.

ELGAR, S.; HERBERS, T.H.C.; CHANDRAN, V., and GUZA, R.T., 1995. Higher order spectral analysis of non linear ocean surface gravity waves. *Journal of Geophysical Research,* 100, 4977–4983.

FAAS, R.W., 1991. Rhelogical boundaries of mud: where are the limits? *Geo-Marine Letters,* 11, 143–146.

FAAS, R.W., 1995. Rheological characteristics of Allepey mud and their role in the formation and maintenance of mudbanks on the Kerala coast of south west of India. *Journal of Coastal Research,* 11, 188–193.

FALQUES, A.; IRANZO, I., and CABALLERIA, M., 1994. Shear instability of longshore currents: effect of dissipation and non-linearity, *Proceedings International Conference Coastal Engineering,* 24, 1983–1997.

GUZA, R.T. and THORNTON, E.B., 1980. Local and shoaled comparisons of sea surface elevations, pressure and velocities. *Journal of Geophysical Research,* 85, 1524–1530.

HUNTLEY, D.A.; GUZA, R.T., and THORNTON, E.B., 1981. Field observations of surf beat 1. Progressive edge waves. *Journal of Geophysical Research,* 86(C7), 6451–6466.

HUNTLEY, D.A.; SIMMONDS, D., and TATAVARTI, R., 1999. Use of collocated sensors to measure coastal wave reflection. *Journal of Waterway, Port, Coastal and Ocean Engineering,* 125(1), 46–52

JIANG, F. and MEHTA, A.J., 1995. Mudbanks of the southwest coast of India—IV: mud visco-elastic properties. *Journal of Coastal Research,* 11(3), 918–926.

KIM, C.S., 1985. Field Observations of Wave Groups and Long Waves on Sloping Beaches. Halifax, Nova Scotia, Canada: Dalhousie University, M.Sc. thesis.

KIM, C.S. and HUNTLEY, D.A., 1985. On time delays in the nearshore zone between onshore and longshore currents at incident wave frequencies. *Journal of Geophysical Research,* 91(C3), 3967–3978.

LI, Y. and PARCHURE, T.M., 1998. Mudbanks of southwest coast of India—VI: suspended sediment profiles. *Journal of Coastal Research,* 14(4), 1363–1372.

MANOJKUMAR, P.; NARAYANA, A.C., and TATAVARTI, R., 1998. Mudbank dynamics: physical properties of sediments. *Journal of Geological Society of India,* 51, 793–798.

MATHEW, J. and BABA, M., 1995. Mudbanks of SW coast of India II: wave-mud interaction, *Journal of Coastal Research,* 11, 178–187.

MATHEW, J.; BABA, M., and KURIEN, N.P., 1995. Mudbanks of SW coast of India I: wave characteristics. *Journal of Coastal Research,* 11, 168–178.

MEHTA, A.J.; and JIANG, F., 1993. Some observations on water wave attenuation over nearshore underwater mudbanks and mudberms. Technical Report of Coastal and Oceanographical Engineering Department, UFL/COEL/MP-93/01, University of Florida, Gainesville, Florida, 45 p.

MEI, C.C.; FAN, S., and JIN, K., 1997. Resuspension and transport of fine sediments by waves. *Journal of Geophysical Research,* 102(C7), 15807–15821.

MEI, C.C.; CHIAN, C., and YE, F., 1998. Transport and resuspension of fine particles in a tidal boundary layer near a small peninsular, *Journal of Physical Oceanography,* 2313–2331.

NAIR, R.R., 1976. Unique mudbanks, Kerala, south west India. *American Association of Petroleum Geologists Bulletin,* 60(4), 616–621.

NARAYANA, A.C.; KUMAR, P.M., and TATAVARTI, R., 2001. Beach dynamics related to the Ambalapuzha mudbank along the south west coast of India. *In*: MCANALLY, W.H., and MEHTA, A.J. (eds.), *Coastal and Estuarine Fine Sediment Processes.* Amsterdam: Elsevier Science B.V., pp. 495–507

OLTMAN-SHAY, J.; HOWD, P.A., and BIRKEMEIR, W.A., 1989. Shear instabilities of the mean longshore current: (2). Field observations. *Journal of Geophysical Research,* 94(C12), 18031–18042.

PUTREVU, U. and SVENDSEN, I.B.A., 1993. Vertical structure of undertow outside the surf zone. *Journal of Geophysical Research,* 98(C12), 22707–22717.

RODRIGUEZ, H.N. and MEHTA, A.J., 1998. Considerations on wave-induced fluid mud streaming at open coasts, *In*: BLACK, K.S., PATERSON, D.M., and CRAMP, A. (eds.), *Sedimentary Processes in the Intertidal Zone,* Volume 139. London: Geological Society, pp. 177–186. Special Publication.

SALLENGER, A.H., 1979. Beach-cusp formation. *Marine Geology,* 56, 23–37.

SHRIRA, V.I.; VORONOVICH, V.V., and KOZHELUPOVA, N.G., 1997. Explosive instability of vorticity waves. *Journal of Physical Oceanography,* 27, 542–554.

SILAS, E.G., 1984. Mudbanks of Kerala-Karnataka—need for an integrated study. *CMFRI Bulletin,* 31, 2–7.

TATAVARTI, R., 1989. The Reflection of Waves on Natural Beaches. Halifax, Nova Scotia, Canada: Dalhousie University, Ph.D. thesis.

TATAVARTI, R.; NARAYANA, A.C.; MANOJ KUMAR, P., and CHAND, S., 1999. Mudbank regime of the Kerala coast during monsoon and nonmonsoon seasons. *Proceedings Indian Academy (Earth and Planetary) Sciences,* 108(1), 57–68.

WELLS, J.T. and KEMP, G.P., 1986. Interaction of surface waves and cohesive sediment: field observations and geologic significance. *In*: MEHTA, A.J. (ed.), *Estuarine Cohesive Sediment Dynamics.* New York: Springer-Verlag, pp. 43–65.